A self-consistent approach for the acoustical modeling of vegetal wools

Clément Piegay, Philippe Gle, Etienne Gourlay, Emmanuel Gourdon, Sandrine Marceau

A self-consistent approach for the acoustical modeling of vegetal wools

Clément Piégay[a,*], Philippe Glé[a], Etienne Gourlay[b], Emmanuel Gourdon[c], Sandrine Marceau[d]

[a] *Cerema, Université Gustave Eiffel, UMRAE - Laboratoire de Strasbourg, 11 rue Jean Mentelin 67035 Strasbourg, France*
[b] *Cerema, BPE Team - Laboratoire de Strasbourg, 11 rue Jean Mentelin 67035 Strasbourg, France*
[c] *Université de Lyon, ENTPE, LTDS UMR CNRS 5513, 3 rue Maurice Audin 69518 Vaulx-en-Velin Cedex, France*
[d] *Université Gustave Eiffel, MAST/CPDM, 77454 Marne-La-Vallée Cedex 2, France*

Abstract

Vegetal wools have the capacity to store atmospheric carbon dioxyde, one of the main gases responsible for climate change. So, these insulating materials are used as key elements for green buildings. Moreover, vegetal wools present high sound absorption level performances contributing to the acoustic comfort of indoor living spaces. These properties are directly related to the morphology and the size of their vegetal fibres. Thus, to take their microstructural specificities into account for the modeling of their sound absorption properties, a micro-macro homogenization approach based on a cylindrical geometry is developed. This modeling method, based on a mix between Homogenization of Periodic Media (HPM) and Self-Consistent Method (SCM), is called SCM_{cyl}. The macroscopic behaviour laws of materials are rigorously obtained by using HPM. Then, the SCM leads to the establishment of two possible analytical solutions (a velocity approach v and a pressure approach p) under the fundamental assumption of the energy equivalence between a generic cylindrical inclusion, representative of the vegetal wools physical and geometrical properties at microscopic scale,

∗. Corresponding author. Tél. :+33 388774652 (Clément Piégay)
Email addresses: clement.piegay@cerema.fr (Clément Piégay), philippe.gle@cerema.fr (Philippe Glé), etienne.gourlay@cerema.fr (Etienne Gourlay), emmanuel.gourdon@entpe.fr (Emmanuel Gourdon), sandrine.marceau@univ-eiffel.fr (Sandrine Marceau)

and the homogeneous equivalent medium at the macroscopic scale. The two modeling approaches developed in this paper, $SCM_{cyl} - v$ and $SCM_{cyl} - p$, can be used to determine the sound absorption of fibrous materials using only two parameters, an equivalent fibre radius value and the material porosity. Finally, these solutions are validated for the vegetal wools case by comparison with experimental measurements.

Keywords: Sound absorption coefficient, Self-consistent method, Homogenization of Periodic Media, Fibrous materials, Vegetal wools

1. Introduction

Vegetal wools provide an innovative and sustainable response to human needs. Indeed, used as vegetal raw materials in green buildings insulation, they bring a significant storage of atmospheric carbon dioxide [1, 2]. In addition, these materials present high levels of performance in sound absorption [3, 4, 5, 6, 7] contributing significantly to the improvement of acoustic comfort inside buildings. Vegetal wools are characterized by the morphological and shape specificities of their fibres. They display a strong variability in fibre size distribution [5, 8]. Moreover, the organization of fibres in the materials leads to an anisotropic behaviour [9, 10]. These aspects of the fibrous microstructure of vegetal wools have a direct impact on their sound absorption performances at macroscopic scale [5, 8, 11, 12, 13] and it is necessary to take them into account when modeling sound absorption coefficient of vegetal wools. To do that, it seems particularly relevant to use real parameters related to fibre geometry and wool structure, such as fibre radius and porosity. Thus, empirical models dedicated to fibrous materials can be used. Some of them such as [14, 15] are approved and widely used in the literature. However, besides not being physically justified, these models historically developed for conventional fibrous materials seem to be less adapted to the high variability of vegetal fibres as shown in [8]. Moreover, they can lead to unphysical predictions as for example negative real parts of complex dynamic density especially at low frequencies [16]. Semi-phenomenological mo-

dels, such as the Johnson-Champoux-Allard-Lafarge model (JCAL) [17, 18, 19], exist and have proven their efficiency for fibrous materials [5, 8] but they usually require five (or more) parameters related to pore configuration. Experimental characterization of some of these parameters such as viscous and thermal characteristic lengths or static thermal permeability is not always possible. So, the work carried out in [20] led to a model limited to three parameters if information on pore size distributions is available. However, semi-phenomenological models have been developed for the geometry of general pore networks and are not directly linked to the microstructural geometry of fibrous media such as fibre sizes which may be an accessible parameter for manufacturers of fibrous insulators. We can then focus on other approaches which are based on homogenization methods that link the properties of an heterogeneous medium at the microstructure scale to the properties of a macroscopic medium. One of the most widely used methods is the Homogenization of Periodic Media (HPM), initially developed by [21, 22]. This modeling method can be applied regardless of the periodic microstructure. However, it requires the implementation of important numerical simulations rather than analytical relationships. This approach has been adapted to the case of fibrous materials in [11, 23], where simplifying assumptions about the representative elementary volume (REV) had to be done in order to decrease the numerical calculations. Other micro-macro approaches are based on 3D modeling of the REV, requiring numerical simulations to determine the sound absorption properties [24]. In [25, 26] an hybrid approach is used on the basis of a numerical homogenization mixed with the JCAL model by numerical calculations related to the finite element method. This approach has been adapted to the case of porous media such as melamine foam in [27] and more recently to the special cases of a glass wool [28] and a vegetal fibrous materials (milkweed fibres) [29]. These methods have several advantages. Indeed, based on a relatively detailed REV, they lead to an accurate modeling of material acoustic properties. Moreover, it is possible to establish relationships between the characteristic parameters of the pore networks related to models such as JCAL and those describing the microstructure of materials. Nevertheless, as this hy-

brid approach requires numerical resolutions, microstructure parameters are not directly related to the macroscopic properties of the materials through analytical relationships. In order to avoid tomography or SEM characterizations, it seems particularly relevant to have direct micro-macro analytical relationships to carry out rapid inverse analyses. To do this, it is possible to use a different but complementary homogenization approach, called Self-Consistent Homogenization (SCM) [30]. It is slightly different from the HPM method. Indeed, the microstructure is not identified with the same precision, but it is reproduced by generic heterogeneities. Also, it is specified in [31] that the fundamental hypothesis of this method is to consider that the material at the macroscopic scale and the microstructural parameters follow the same behaviour laws. In the case of a spherical geometry, coupled HPM-SCM approach has been developed in dynamics by [32, 33]. The HPM method is used to rigorously obtain the macroscopic behaviour laws of materials. The SCM approach is applied in a second step by relying on a two-component spherical inclusion (solid phase included in the fluid phase) in order to obtain relationships directly linking microstructural parameters such as spherical grain sizes and macroscopic properties. However, this method based on a spherical geometry is mainly dedicated to granular materials. For fibrous materials having a cylindrical geometry, Boutin's work [34] has been limited to a static approach based on [35]. However, another SCM modeling approach has been developed in the literature, but without the fundamental self-consistent assumption, for example for a spherical geometry by [36]. For a cylindrical geometry, the Tarnow model is frequently used in the literature for modeling the sound absorption properties of fibrous materials [37, 38, 39]. Thus, in the light of all the above components and in order to directly relate both the fibre characteristic parameters and the material structure to their macroscopic properties, it seems particularly relevant to develop a cylindrical Self-Consistent Modeling approach in dynamic (SCM_{cyl}). Indeed, on the basis of the laws of macroscopic behaviour established by HPM, as in C. Boutin spherical approach, this SCM_{cyl} approach can lead to possible analytical solutions between specific parameters of fibrous microstructural media and macroscale sound absorption

properties. Moreover, it can take the anisotropic nature of vegetal wools into account, while respecting the fundamental hypothesis of energy conservation. Therefore, this paper is organised as follows : Section 2 describes very synthetically the determination of macroscopic behaviour laws by HPM approach. Then, after presenting assumptions about the representative elementary volume, the SCM_{cyl} approach is exposed. In Section 3, the SCM_{cyl} modeling approach is validated by comparison with experimental data on two vegetal wools. Finally, in section 4, these results and the hypothesis done for the SCM_{cyl} developments are discussed by way of conclusion.

2. Modeling

2.1. Macroscopic laws from the HPM

The description of this method is widely available in the literature, especially for the general case of porous materials [32, 40, 41]. Thus, after a description of the hypotheses and simplifications made in the present case for a fibrous medium, the HPM main steps and results are recalled.

2.1.1. Basic hypothesis concerning the fibrous medium

We consider a biphasic fibrous medium composed by a solid phase (Ω_s) and a fluid phase (Ω_f) saturating this medium. As a first approximation and to take its anisotropic nature into account, the solid phase is represented by fibres of constant cross-section over their entire length (which is considered large in comparison with the cross-section size) [42]. Moreover, in our case, this medium is represented by a regular layout of the fibres which are parallel to each other, as shown by Fig. 1. In the general case, the solid phase is considered elastic [43], [44]. Nevertheless, the work carried out in [45] defines a decoupling frequency (f_d) above which it can be considered that only a compression wave propagates in the fluid phase. Then, in this case, the hypothesis of a rigid solid phase is acceptable. So, this assumption is used as a first approximation for the solid phase. Moreover, this phase is considered impermeable and its thermodynamic

evolution is considered isothermal. The fluid phase is considered as a Newtonian viscous and compressible fluid of viscosity μ and thermal conductivity λ_f (air thermal conductivity). The porosity ϕ is considered to be open and the porous network is interconnected. Moreover, the case of a single porosity medium is chosen and wavelengths are considered large in comparison with the pore sizes in order to neglect diffraction effects.

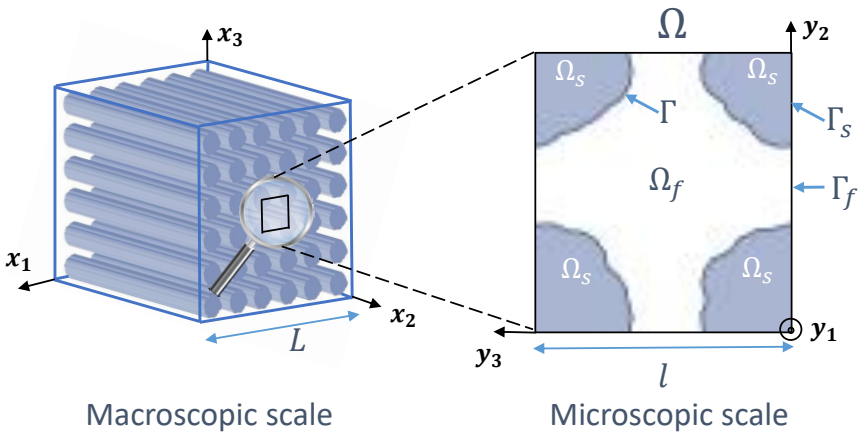

FIGURE 1: Schematic representation of a fibrous medium at macroscopic and microscopic scales by the periodic cell Ω. Ω_s and Ω_f correspond to volumes of the solid and fluid phases. Γ is the solid-fluid interface. Γ_s and Γ_f are the solid and fluid interfaces with the cell boundary Ω

Two specific orientations can be considered for the acoustic excitation. The first one is in a plane defined by $(\mathbf{x_1}, \mathbf{x_3})$, perpendicular to the longitudinal axis $(\mathbf{x_2})$ of fibres. The second limit case corresponds to an acoustic excitation parallel to the longitudinal axis of the fibre $(\mathbf{x_2})$. However, the parallel case does not correspond to a conventional use of insulation panels in buildings. Even though all orientations of the wave are possible between these two limits [9, 29], in this paper, only a specific focus is done on the perpendicular case which corresponds to most practical applications. To use a micro-macro homogenization method, two basic principles must be respected :

— the existence of a representative elementary volume (REV) ;

— the scale separation between the medium macroscopic representation and the microscopic characteristics of heterogeneities.

So, as shown by Fig. 1, the REV is related to the microscopic length (l) and the fibrous medium is associated to the macroscopic length (L). Both lengths are related to the scale ratio $\varepsilon = \frac{l}{L} \ll 1$. The acoustic solicitation is represented by the propagation of a harmonic plane wave of velocity c_0 and of unit amplitude in the fibrous medium. Then, this wave is subjected to dissipation phenomena related to both visco-inertial and thermal effects. It is possible to establish local-level relationships for each of these phenomena.

2.1.2. Basic equations related to visco-inertial and thermal effects

An acoustic wave propagates through the fluid phase. The wave is considered harmonic ($e^{j\omega t}$ dependency is supposed, with $j^2 = -1$ and $\omega = 2\pi f$ is the angular frequency, f being the frequency in hertz), so the linearized Navier-Stokes equation governing the fluid phase is written :

$$\mu \Delta \mathbf{v} - \nabla p = j\omega \rho_0 \mathbf{v} \tag{1}$$

with μ the dynamic viscosity, $\mathbf{v}$ the local speed of the fluid, p the pressure and ρ_0 the fluid phase bulk density at rest.

The local form of the linearized mass conservation equation is given by the following relationship :

$$j\omega \rho + \rho_0 \nabla . \mathbf{v} = 0 \tag{2}$$

with ρ the bulk density.

At the local scale, the temperature variation is governed by the linearized heat equation, which is expressed by the relation :

$$\lambda_f \Delta T - j\omega \rho_0 C_p T = -j\omega p \tag{3}$$

with λ_f the thermal conductivity of the fluid phase, T the temperature and C_p the heat capacity at constant pressure.

2.1.3. Scale separation condition

The next step of HPM is the scale separation condition. It consists in scaling each term of the linearized equations (Eqs. 1 to 3). To do that, we define the variable $\mathbf{X}$. It can be related to the variable $\mathbf{x} = \frac{\mathbf{X}}{L}$ at macroscopic scale and to the variable $\mathbf{y} = \frac{\mathbf{X}}{l}$ at microscopic scale. $\mathbf{x}$ and $\mathbf{y}$ are related to ε by the following relationship : $\mathbf{x} = \varepsilon\mathbf{y}$. Then, each vector and scalar field, $\mathbf{v}$, p, ρ and T can be expressed as an asymptotic development in powers of ε as follows : $f(\mathbf{x},\mathbf{y}) = \sum_{i=0}^{\infty} \varepsilon^i f^i(\mathbf{x},\mathbf{y})$. The gradient ($\nabla$), divergence ($\nabla.$) and Laplacian ($\Delta$) operators are approximated by the following relationships : $\nabla \simeq \nabla_{\mathbf{x}} + \varepsilon^{-1}\nabla_{\mathbf{y}}$; $\nabla. \simeq \nabla_{\mathbf{x}}. + \varepsilon^{-1}\nabla_{\mathbf{y}}.$; $\Delta \simeq \Delta_x + 2\varepsilon^{-1}\nabla_{\mathbf{x}}.\nabla_{\mathbf{y}}$. After injecting the asymptotic developments into the equations relating to viscous and thermal dissipation phenomena, terms of the same order can then be identified. At the order $o(\varepsilon^{-1})$, we obtain the following relationships :

$$\nabla_{\mathbf{y}} p^0 = 0 \tag{4}$$

The pressure is uniform in the pores at the first order. So, it can be expressed by : $p^0 = p^0(\mathbf{x}) = P$. We also find the hypothesis of incompressibility of the fluid, in the first order, at the pore scale :

$$\nabla_{\mathbf{y}}.\mathbf{v}^0 = 0 \tag{5}$$

At the order $o(1)$, we obtain the following relationships :

— Visco-inertial effects

$$\begin{cases} \mu\Delta_y \mathbf{v}^0 - \nabla_{\mathbf{y}} p^1 - \nabla_{\mathbf{x}} p^0 = j\omega\rho_0 \mathbf{v}^0 & (6) \\ j\omega\rho^0 + \nabla_{\mathbf{y}}.\mathbf{v}^1 + \nabla_{\mathbf{x}}.\mathbf{v}^0 = 0 & (7) \end{cases}$$

— Thermal effects

$$\{ \quad \lambda_f \Delta_y T^0 - j\omega\rho_0 C_p T^0 = -j\omega p^0 \tag{8}$$

2.1.4. Variational formulation resolution and energy conservation condition

The resolution of the previous set of equations is traditionally realized in the literature using a variational formulation. This mathematical operation consists

in performing the scalar product of each terms by a $\mathbf{w}$ field belonging to the vector space W, defined by : $W = \{\mathbf{w}, \Omega - periodic \,/\, \nabla_{\mathbf{y}}.\mathbf{w} = 0, \mathbf{w}_{/\Gamma} = \mathbf{0}\}$. Equations are then integrated over Ω_f. For the visco-inertial effects, based on Eq. 6 we can express the following relationship :

$$-\iiint_{\Omega_f} \nabla_{\mathbf{y}} p^1.\mathbf{w}\mathrm{d}\Omega + \mu \iiint_{\Omega_f} \Delta_y \mathbf{v}^0.\mathbf{w}\mathrm{d}\Omega - \iiint_{\Omega_f} \nabla_{\mathbf{x}} p^0.\mathbf{w}\mathrm{d}\Omega = \iiint_{\Omega_f} j\omega\rho_0 \mathbf{v}^0.\mathbf{w}\mathrm{d}\Omega \tag{9}$$

To simplify Eq. 9, we use the flow-divergence theorem showing an equality between the integral on a given volume (V) of the vector field ($\mathbf{F}$) divergence and the flow of this field through the surface ($\mathrm{d}S$) representing the volume boundary (∂V). By associating a scalar field (g) to the vector field ($\mathbf{F}$), we can write this theorem :

$$\iiint_V (\mathbf{F}.\nabla g + g\,(\nabla \cdot \mathbf{F}))\,\mathrm{d}V = \oiint_{\partial V} g\mathbf{F} \cdot \mathbf{dS} \tag{10}$$

Based on this theorem, as well as the periodicity properties of the functions belonging to the vector space W and assuming that $\overrightarrow{w} = \overline{\mathbf{v}^0}$, the conjugate of the velocity $\mathbf{v}^0$, we obtain the following relation :

$$\iiint_{\Omega_f} \nabla_{\mathbf{y}} \mathbf{v}^0 \cdot \nabla_{\mathbf{y}} \overline{\mathbf{v}^0} \mathrm{d}\Omega + j\frac{\omega\rho_0}{\mu} \iiint_{\Omega_f} \mathbf{v}^0 \cdot \overline{\mathbf{v}^0} \mathrm{d}\Omega = -\frac{1}{\mu} \nabla_{\mathbf{x}} P \iiint_{\Omega_f} \overline{\mathbf{v}^0} \mathrm{d}\Omega \tag{11}$$

This relationship demonstrates the energy conservation between the microscopic and macroscopic descriptions of the fibrous medium, which is a fundamental assumption of homogenization models. Then, the solution is classically written :

$$\mathbf{v}^0(\mathbf{x}, \mathbf{y}, \omega) = -\frac{[\pi(\mathbf{y}, \omega)]}{\mu} \nabla_{\mathbf{x}} P(\mathbf{x}, \omega) \tag{12}$$

$\pi(\mathbf{y}, \omega)$ represents the local permeability tensor. By integrating $\mathbf{v}^0(\mathbf{x}, \mathbf{y}, \omega)$ over Ω, we get the macroscopic velocity of the equivalent homogeneous medium :

$$\langle \mathbf{v}^0 \rangle_\Omega = -\frac{[\Pi(\omega)]}{\mu} \nabla_{\mathbf{x}} P(\mathbf{x}, \omega) \tag{13}$$

This equation corresponds to the **Generalized Darcy's Law**, where $[\Pi(\omega)]$ is the dynamic permeability tensor related to the dynamic density ρ with the following relation : $\rho(\omega) = \frac{\mu}{j\omega\Pi(\omega)}$.

For the thermal effect, applying the same procedure as for visco-inertial effects, Eq. 8 leads to the following relationship :

$$\lambda_f \iiint_{\Omega_f} \nabla_{\mathbf{y}} T^0 \cdot \nabla_{\mathbf{y}} \overline{T^0} \mathrm{d}\Omega + j\omega\rho_0 C_p \iiint_{\Omega_f} T^0 \overline{T^0} \mathrm{d}\Omega = j\omega P \iiint_{\Omega_f} \overline{T^0} \mathrm{d}\Omega \quad (14)$$

This relationship represents the energy conservation for heat dissipation effects between the local scale represented by the terms on the left and the equivalent homogeneous medium, macroscopic scale, represented by the right term. The solution of the variational formulation process is expressed according to the following relationship where $\xi(\mathbf{y}, \omega)$ represents the thermal permeability at the local scale :

$$T^0(\mathbf{x}, \mathbf{y}) = \frac{\xi(\mathbf{y}, \omega)}{\lambda_f} j\omega P(\mathbf{x}, \omega) \quad (15)$$

The relation governing the macroscopic temperature variation of the equivalent homogeneous medium is obtained by integrating over Ω :

$$\langle T^0 \rangle_\Omega = \frac{\Xi(\omega)}{\lambda_f} j\omega P(\mathbf{x}) \quad (16)$$

Eq. 16 is equivalent to Darcy's law for visco-inertial effects. $\Xi(\omega)$ is the dynamic thermal permeability of the equivalent homogeneous medium. It is related to the bulk modulus K with the following relation : $K(\omega) = \frac{\gamma P_0/\phi}{\gamma - j(\gamma-1)\frac{\Xi(\omega)}{\delta_t^2 \phi}}$.

Using the HPM approach, relationships can be established between the local velocity, pressure and temperature fields and their macroscopic shape related to the equivalent homogeneous medium. However, the HPM is used independently of the morphology of the elementary cell and the implementation of numerical resolutions is necessary to determine solutions. Thus, in order to determine possible analytical solutions, a coupling of the HPM and the SCM homogenization is performed. To do that, SCM is used on the basis of the equations governing the laws of behaviour on a macroscopic scale that have been established in this section and on the fundamental hypothesis of energy conservation.

2.2. SCM with cylindrical geometry (SCM_{cyl}) adapted to fibrous media

This method has been used in static for the determination of ρ, for fibrous materials by [35] and for granular materials (spherical SCM) by [34]. Subsequently, work carried out in [32] and [33] led to the determination of ρ and of

the bulk modulus K in dynamic, but only in the case of the granular materials with spherical geometry. To apply this method, it is first necessary to develop a generic inclusion of simplified geometry and to establish the equations governing the behaviour of the velocity, local pressure and temperature fields. Then, under the constraint of an homogeneous macroscopic force, differential equations are obtained and solved to determine solutions for the three characteristic quantities within the fluid phase. Then, the establishment of boundary conditions makes it possible to propose two families of possible solutions for ρ and K, which can be used for the modeling of fibrous materials acoustic properties.

2.2.1. Cylindrical generic inclusion for a fibrous medium

The selected generic inclusion (Ω) is a biphasic inclusion described by a cylinder of radius (R) and surface (∂R). The solid phase, representative of a fibre of volume (Ω_s), has a radius (βR) constant along its entire length (Z) considered, in first approximation, large in comparison with the cylinder cross-section ($\frac{Z}{r} = \varepsilon \ll 1$). The solid phase is included in an air cylinder (fluid phase) with a hole in the middle. Its external radius is R and its internal radius is βR, as shown in Fig. 2. Thus, we can express the porosity ϕ from the solid phase radii βR and the inclusion R. $\phi = 1 - \left(\frac{\beta R}{R}\right)^2 = 1 - \beta^2$. The macroscopic stress materialized by a pressure gradient $\nabla \mathbf{P}$, has been represented in Fig. 2 in a plane defined by $(\mathbf{e_r}, \mathbf{e}_\theta)$, perpendicular to the longitudinal axis ($\mathbf{e_z}$) of the fibres. As indicated in section 2.1.1, only this special limit case is investigated. To simplify the writing of the acoustic pressure force, $\nabla \mathbf{P}$ is replaced by a force noted $\mathbf{G} = \nabla \mathbf{P}$. So, at macroscopic scale in the equivalent homogeneous medium, generalized Darcy law for the visco-inertial effects and equivalent Darcy law for the thermal effects are expressed through the following relationships :

$$\langle \mathbf{v} \rangle = \mathbf{V} = -\frac{\Pi}{\mu} \nabla \mathbf{P} = -\frac{\Pi}{\mu} \mathbf{G} \tag{17}$$

$$\langle T \rangle = \frac{\Xi}{\lambda_f} j\omega P \tag{18}$$

In the fluid phase of the cylindrical inclusion for $\beta R < r < R$:

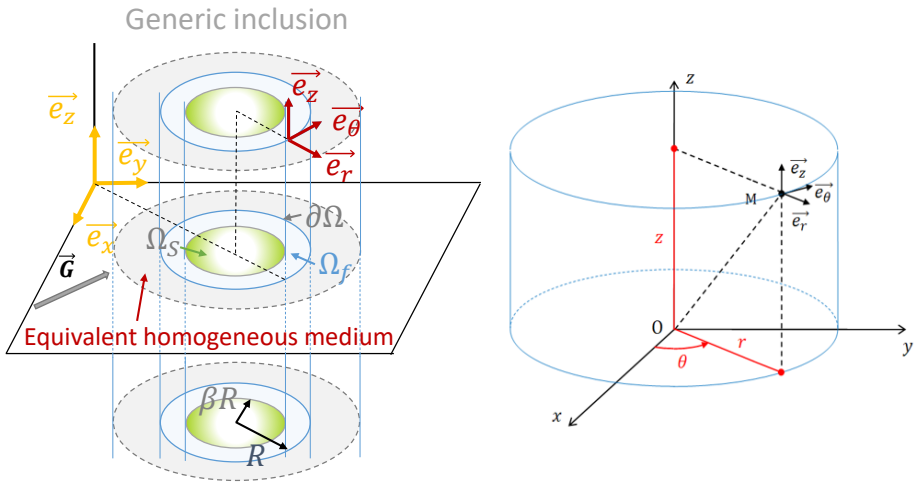

FIGURE 2: Schematic representation of a fibrous medium at macroscopic and microscopic scales by the periodic cell Ω. Ω_s and Ω_f correspond to volumes of the solid and fluid phases. Γ is the solid-fluid interface. Γ_s and Γ_f are the solid and fluid interfaces with the cell boundary Ω

— local fluid movements are governed by the linearized Navier-Stokes equation. For convenience, it is expressed as :

$$-\nabla p - \frac{1}{\delta_v^2}\mu\mathbf{v} + \Delta(\mu\mathbf{v}) = \mathbf{0} \tag{19}$$

with $\delta_v = \sqrt{\frac{\mu}{j\rho_0\omega}}$ the viscous boundary layer thickness ;

— based on Eq. 5 the fluid phase is considered as incompressible at the first order :

$$\nabla.\mathbf{v} = 0 \tag{20}$$

— no slip condition between the solid phase and the fluid phase is zero :

$$\mathbf{v}_{/\Gamma} = \mathbf{0} \tag{21}$$

— temperature field variations in the fluid phase are governed by the linearized heat equation which is expressed as follows :

$$\Delta T - \frac{1}{\delta_t^2}T + \frac{j\omega P}{\lambda_f} = 0 \tag{22}$$

With $\delta_t = \sqrt{\frac{\lambda_f}{\rho_0 C_p \omega}}$ the thermal boundary layer thickness ;

— the temperature condition at the solid/fluid interface is zero :

$$T_{/\Gamma} = 0 \tag{23}$$

2.2.2. The pressure field

In a first approximation and based on [46] works, which is also used in [32], it is possible to expressed the pression field (p) as a function of both $\mathbf{G}$ and a function denoted h (which has to be determined) depending on r by the following relationship :

$$p = \mathbf{G}.\nabla \mathbf{h}(r) \tag{24}$$

Using the divergence operator ($\nabla.$) on the linearized Navier-Stokes equation (Eq. 19), we get :

$$\nabla.\nabla p - \frac{1}{\delta_v^2}\mu \nabla.\mathbf{v} + \omega\left(\mu \nabla.\mathbf{v}\right) = 0 \tag{25}$$

However, as the fluid is considered incompressible at the local scale (Eq. 20), the previous expression (Eq. 25) can be simplified and we can write it :

$$\Delta p = 0 \tag{26}$$

By combining Eqs. 24 and 26, we obtain :

$$\Delta\left(\mathbf{G}.\nabla \mathbf{h}(r)\right) = \mathbf{G}.\nabla(\Delta h(r)) = G_r \frac{\partial(\Delta h(r))}{\partial r} = 0 \tag{27}$$

Then, it leads to the following differential equations :

$$\Delta h(r) = c_0 \tag{28}$$

Finally, the expression of h function can be obtained by the following relationship :

$$h(r) = c_0 \ln(r) + \frac{c_1 . r^2}{4} \tag{29}$$

The constant term is taken equal to zero because it has no physical meaning and it does not participate in the establishment of boundary conditions.

2.2.3. The velocity field

As for the case of the scalar field p, it is possible to rely on [32, 46] to express the local velocity vector field in the following form :

$$\mu \mathbf{v} = \mathbf{G}\left[\nabla \otimes \nabla f(r) + g(r) I\right] \tag{30}$$

with $\otimes$ representing the tensor product operator and I the identity matrix. Applying the divergence operator to Eq. 30, we obtain the following relationship :

$$\mathbf{G}.\nabla.\left[\nabla \otimes \nabla f(r) + g(r) I\right] = \mu \nabla.\mathbf{v} = 0 \tag{31}$$

Then, Eq. 31 can be written in the following form :

$$\mathbf{G}.\nabla\left[\Delta f(r) + g(r)\right] = G_r\left(\frac{\partial(\Delta f(r) + g(r))}{\partial r}\right) = 0 \tag{32}$$

Thus, we can write that $\Delta f(r) + g(r) = a_0$, or $g(r) = -\Delta f(r) + a_0$ with a_0 a constant. By injecting the $g(r)$ expression into Eq. 30, we obtain the following relationship :

$$\mu \mathbf{v} = \mathbf{G}\left[\nabla \otimes \nabla f(r) - \Delta f(r) I + a_0 I\right] \tag{33}$$

On the other hand, we can include the term $-\frac{a_0}{2} r^2$ in the $f(r)$ function in order to remove the term $a_0 I$. Eq. 30 is finally written :

$$\mu \mathbf{v} = \mathbf{G}.\left[\nabla \otimes \nabla f(r) - \Delta f(r) I\right] \tag{34}$$

Now, we can replace both $\mu \mathbf{v}$ and p terms in the linearized Navier-Stokes equation (Eq 19) by their respectively expressions given by both Eq 24 and Eq 34. Thus, we obtain the following relationship :

$$-\nabla.(\mathbf{G}.\nabla h(r)) - \frac{1}{\delta_v^2}\mathbf{G}.\left[\nabla \otimes \nabla f(r) - \Delta f(r) I\right] + \Delta\left(\mathbf{G}.\left[\nabla \otimes \nabla f(r) - \Delta f(r) I\right]\right) = \mathbf{0} \tag{35}$$

This expression can also be written in the following simplified form :

$$-\mathbf{G}.\Delta h(r) I + \mathbf{G}.\left[\nabla \otimes \nabla - I\Delta\right]\left[-h(r) + \Delta f(r) - \frac{1}{\delta_v^2} f(r)\right] = \mathbf{0} \tag{36}$$

To further simplify Eq. 36, a m function is introduced. It is expressed by : $m(r) = \left[-h(r) + \Delta f(r) - \frac{1}{\delta_v^2} f(r)\right]$. Moreover, the h function is replaced by its

expression given by Eq. 29. So, $\Delta h(r) = \frac{1}{r}\frac{\partial}{\partial r}\left(r\frac{\partial h}{\partial r}\right) = c_1$. Finally, Eq. 36 can be written :

$$\mathbf{G}.\left[-c_1 I + \nabla \otimes \nabla m(r) - I\Delta m(r)\right] = \mathbf{0} \tag{37}$$

with $\nabla \otimes \nabla m(r) = \begin{bmatrix} \frac{\partial}{\partial r}\left(\frac{\partial m(r)}{\partial r}\right) & 0 & 0 \\ 0 & \frac{1}{r}\frac{\partial m(r)}{\partial r} & 0 \\ 0 & 0 & 0 \end{bmatrix}$ and $\Delta m(r) = \frac{1}{r}\frac{\partial m(r)}{\partial r} + \frac{\partial^2 m(r)}{\partial r^2}$.

Eq. 37 can thus be written in matrix form as follows :

$$\mathbf{G}.\begin{bmatrix} -c_1 - \frac{1}{r}\frac{\partial m(r)}{\partial r} & 0 & 0 \\ 0 & -c_1 - \frac{\partial^2 m(r)}{\partial r^2} & 0 \\ 0 & 0 & -c_1 - \frac{\partial^2 m(r)}{\partial r^2} - \frac{1}{r}\frac{\partial m(r)}{\partial r} \end{bmatrix} = \mathbf{0} \tag{38}$$

So, $\frac{\partial m(r)}{\partial r} = -c_1 r$. Thus, we can express the m function by the following expression :

$$m(r) = -h(r) + \Delta f(r) - \frac{1}{\delta_v^2} f(r) = -c_0 \ln(r) - \frac{c_1}{4} r^2 + \Delta f(r) - \frac{1}{\delta_v^2} f(r) = -\frac{c_1}{2} r^2 \tag{39}$$

Finally, for the function f, we obtain a second degree differential equation with non-constant coefficients and with a second member. It is expressed by the following relation :

$$\frac{\partial^2 f(r)}{\partial r^2} + \frac{1}{r}\frac{\partial f(r)}{\partial r} - \frac{1}{\delta_v^2} f(r) = c_0 \ln(r) - \frac{c_1}{4} r^2 \tag{40}$$

The solution is :

$$f(r) = \delta_v^2 \left(-c_0 \ln r + \frac{c_1}{4} r^2 - c_1 \delta_v^2\right) + c_2 I_0(r/\delta_v) + c_3 K_0(r/\delta_v) \tag{41}$$

With I_0 and K_0, modified Bessel functions of the first species.

2.2.4. The temperature field

By analogy with visco-inertial effects and by using the equations previously established for heat dissipation in Section 2.1.4, the temperature T can be expressed as a function of local scale thermal permeability by the following relationship :

$$T(r) = \xi(r)\frac{j\omega P}{\lambda_f} \tag{42}$$

By injecting this T expression into Eq. 22, we obtain the following relationship :

$$\Delta\xi(r) - \frac{1}{\delta_t^2}\xi(r) + 1 = 0 \tag{43}$$

By expressing $\Delta\xi(r)$ in cylindrical coordinates, we finally obtain the following differential equation :

$$\frac{\partial^2\xi(r)}{\partial r^2} + \frac{\partial\xi(r)}{\partial r} - \frac{1}{\delta^2}\xi = -1 \tag{44}$$

The solution of this equation is :

$$\xi(r) = \delta_t^2 + c_4 I_0(r/\delta_t) + c_5 K_0(r/\delta_t) \tag{45}$$

The expressions of the functions relating to the pressure, velocity and temperature fields have been expressed locally. It is now necessary to determine the five constants used in these functions. To do that, we can use the boundary conditions of the problem. First, concerning the velocity, boundary conditions can be expressed at the solid-fluid boundary as well as at the inclusion boundary. Then, concerning the pressure, strains on generic inclusion at the inclusion boundary should also be expressed. In addition, concerning the temperature, boundary conditions can be expressed at the solid-fluid interface too. Finally, it is necessary to take the energy conservation condition between inclusion, at the local scale, and the equivalent homogeneous medium into account for both visco-inertial and thermal effects.

2.2.5. Boundary conditions at the solid-fluid interface

At the solid-fluid interface, $r = \beta R$, no slip condition (Eq. 21) leads to a zero velocity, $\mathbf{v}(\beta R) = \mathbf{0}$ and the temperature variation condition (Eq. 23) also leads to zero. This condition concerning the temperature variation allows us to easily and quickly establish the first boundary condition. Indeed, it can be expressed by the following relationship :

$$\xi(\beta R) = 0 \tag{46}$$

Concerning the velocity, based on both the cylindrical geometry and the hypothesis of a perpendicular flow (in the plane $(\mathbf{e_r}, \mathbf{e}_\theta)$), it can be written $\mathbf{v} =$

$v_r\mathbf{e_r} + v_\theta \mathbf{e}_\theta$. Thus, based on Eq. 34, the velocity can be written as the following relationship :

$$\begin{pmatrix} \mu v_r \\ \mu v_\theta \\ 0 \end{pmatrix} = \begin{pmatrix} G\cos\theta \\ G\sin\theta \\ 0 \end{pmatrix} \begin{bmatrix} -\frac{1}{r}\frac{\partial f(r)}{\partial r} & 0 & 0 \\ 0 & -\frac{\partial^2 f(r)}{\partial r^2} & 0 \\ 0 & 0 & -\frac{1}{r}\frac{\partial f(r)}{\partial r} - \frac{\partial^2 f(r)}{\partial r^2} \end{bmatrix} \tag{47}$$

Thus, we obtain two relationships for the velocity vector at the local scale, projected on $(\mathbf{e_r}, \mathbf{e}_\theta)$:

— On the $\mathbf{e_r}$ axis :

$$\mu v_r(r) = -G\cos\theta \frac{1}{r}\frac{\partial f(r)}{\partial r} \tag{48}$$

— On the $\mathbf{e}_\theta$ axis :

$$\mu v_\theta(r) = -G\sin\theta \frac{\partial^2 f(r)}{\partial r^2} \tag{49}$$

In combination with no slip condition and Eqs. 48, 49, we obtain the second and the third boundary conditions :

$$-\frac{1}{\beta R}\frac{\partial f(\beta R)}{\partial r} = 0 \tag{50}$$

$$-\Delta f(\beta R) = 0 \tag{51}$$

To summarize, the three boundary conditions for local velocity and temperature are given by Eqs.46, 50 and 51.

2.2.6. Boundary conditions at the inclusion frontier

It is also possible to express a boundary velocity condition between the generic inclusion and the equivalent homogeneous medium ($r = R$). Indeed, the mean velocity within the inclusion is equal to the macroscopic velocity given by the Darcy relation expressed by Eq. 17. This equality leads to the following relationship :

$$\mathbf{V}(r) = \frac{1}{\Omega}\iiint_{\Omega_f} \mathbf{v}(r)\mathrm{d}\Omega \tag{52}$$

It is possible to rewrite Eq. 52 as the following expression :

$$\iiint_{\Omega_f} \mathbf{v}(r)\mathrm{d}\Omega = \iiint_{\Omega_f} \left(\mathbf{v}.\nabla r\mathbf{e_r} + r\mathbf{e_r}\left(\nabla\cdot\mathbf{v}(r)\right)\right)\mathrm{d}\Omega \tag{53}$$

Indeed, $\nabla r \cdot \mathbf{e_r} = 1$ and $\nabla.\mathbf{v} = 0$ (Eq. 20). Then, we can simplify this expression by using the relation of the flow-divergence theorem exposed earlier by Eq. 10 :

$$\iiint_{\Omega_f} \mathbf{v}(r)\mathrm{d}\Omega = \oiint_{\partial\Omega} r\mathbf{e_r} \cdot \mathbf{v}(r) \cdot \mathbf{dS} \tag{54}$$

for $r = R$, $\mathbf{dS} = R\,\mathrm{d}\theta\,\mathrm{d}z\,\mathbf{e_r}$. Finally, by solving the surface integral, the mean velocity can be obtained :

$$\mathbf{V}(r) = \frac{1}{\mu\,R}\frac{\partial f(R)}{\partial r}\mathbf{G} \tag{55}$$

By identifying $\mathbf{V}(r)$ with the Generalized Darcy Equation 17, we can write a third boundary condition for $r = R$ as a function of the permeability Π, by the following relationship :

$$-\frac{1}{R}\frac{\partial f(R)}{\partial r} + \Pi = 0 \tag{56}$$

The normal fluid velocity $v_r(r)$ is expressed as a function of $\frac{\partial f(r)}{\partial r}$. So, this boundary condition means that radial velocities are equal at any point on the frontier surface between the inclusion and the equivalent homogeneous medium. Thus, we can write the following relation :

$$v_r(R) = V_r(R) \tag{57}$$

Now, on the basis of [32, 33], we can express the stress on generic inclusion at the inclusion boundary. So, it is physically possible to implement an equality between the pressure P in the equivalent homogeneous medium and the inclusion stress, which can be expressed as $-p\mathbf{I} + 2\,\mu\,\underline{\mathbf{D}}\,(\mathbf{v}(r))$ with $\underline{\mathbf{D}}\,(\mathbf{v}(r))$ the tensor of the deformation rates depending on the local velocity. This condition can be written :

$$\oiint_{\partial\Omega} \left[-(p-P)\mathbf{I} + 2\,\mu\,\underline{\mathbf{D}}\,(\mathbf{v}(r))\right] \cdot \mathbf{dS} = 0 \tag{58}$$

At the inclusion frontier, $r = R$, $\mathbf{dS} = R\,\mathrm{d}\theta\,\mathrm{d}z\,\mathbf{e_r}$. The integral of the three terms forming Eq. 58 can be calculated separately. The first term is $\oiint_{\partial\Omega} -p\,\mathbf{I}\cdot\mathbf{dS}$. Using the expression for p given by Eq. 24, we can write $\oiint_{\partial\Omega} -p\,\mathbf{I}\,\mathbf{dS} = \oiint_{\partial\Omega} -\mathbf{G} \cdot \nabla h(r) \cdot \mathbf{I} \cdot \mathbf{dS}$. So, the result is given by the following relationship :

$$\oiint_{\partial\Omega} -p\mathbf{I}\mathbf{dS} = -\pi R Z \frac{\partial h(R)}{\partial r} G \tag{59}$$

with Z the cylindrical inclusion height which will later vanish. Now, to resolve the second integral, we can use the flow-divergence theorem presented by Eq. 10. Thus, $\oiint_{\partial\Omega} P\,\mathbf{I}\,\mathbf{dS} = \iiint_{\Omega_f} (\mathbf{I}\cdot\nabla P + P\nabla.\mathbf{I})\,\mathrm{d}\Omega$. With $\nabla.\mathbf{I} = 0$, $\nabla P = \mathbf{G}$ and $\mathrm{d}\Omega = r\,\mathrm{d}r\,\mathrm{d}\theta\,\mathrm{d}z$. So, the result is given by the following relationship :

$$\oiint_{\partial\Omega} P\,\mathbf{I}\,\mathrm{d}\mathbf{S} = \pi R^2 Z G \tag{60}$$

Finally, to obtain the third term of Eq. 58, it is necessary to use the tensor $\underline{\mathbf{D}}\,(\mathbf{v}(r))$ based on the expressions of $v_r(r)$ (Eq. 48) and $v_\theta(r)$ (Eq. 49). The expression of $2\,\mu\,\underline{\mathbf{D}}\,(\mathbf{v}(r))$ is given by the following relationship :

$$2\mu\underline{\mathbf{D}}\,(\mathbf{v}(r)) = \begin{bmatrix} -2(\mathbf{G}\cdot\mathbf{e_r})\frac{\partial}{\partial r}\left(\frac{1}{r}\frac{\partial f(r)}{\partial r}\right) & (\mathbf{G}\cdot\mathbf{e}_\theta)\left(\frac{1}{r}\frac{\partial^2 f(r)}{\partial r^2} - \frac{\partial^3 f(r)}{\partial r^3}\right) & 0 \\ (\mathbf{G}\cdot\mathbf{e}_\theta)\left(\frac{1}{r}\frac{\partial^2 f(r)}{\partial r^2} - \frac{\partial^3 f(r)}{\partial r^3}\right) & -2(\mathbf{G}\cdot\mathbf{e_r})\frac{1}{r^2}\frac{\partial f(r)}{\partial r} & 0 \\ 0 & 0 & 0 \end{bmatrix} \tag{61}$$

for $r = R$, $\mathbf{dS} = \mathrm{d}S\,\mathbf{e_r} = R\,\mathrm{d}\theta\,\mathrm{d}z\,\mathbf{e_r}$. So, we can write :

$$\oiint_{\partial\Omega} 2\mu\underline{\mathbf{D}}\,(\mathbf{v}(R))\cdot\mathbf{e_r}\mathrm{d}S = \oiint_{\partial\Omega} 2\mu D_{rr}\mathrm{d}S + \oiint_{\partial\Omega} 2\mu D_{r\theta}\mathrm{d}S \tag{62}$$

with

$$\begin{cases} 2\mu D_{rr} = -2G\cos\theta\dfrac{\partial}{\partial r}\left(\dfrac{1}{r}\dfrac{\partial f(r)}{\partial r}\right) & (63) \\ 2\mu D_{r\theta} = G\sin\theta\left(\dfrac{1}{r}\dfrac{\partial^2 f(r)}{\partial r^2} - \dfrac{\partial^3 f(r)}{\partial r^3}\right) & (64) \end{cases}$$

Thus, we obtain the following result :

$$\oiint_{\partial\Omega} 2\mu\underline{\mathbf{D}}\,(\mathbf{v}(r))\cdot\mathbf{e_r}\mathrm{d}S = \pi RZG\left(-\frac{\partial^3 f(R)}{\partial r^3} + \frac{1}{R}\frac{\partial^2 f(R)}{\partial r^2} - 2\frac{\partial}{\partial r}\left(\frac{1}{R}\frac{\partial f(R)}{\partial r}\right)\right) \tag{65}$$

Finally, we can can write the solution by the following relationship :

$$\oiint_{\partial\Omega} 2\mu\underline{\mathbf{D}}\,(\mathbf{v}(r))\cdot\mathbf{e_r}\mathrm{d}S = \pi RZG\left(-\frac{\partial}{\partial r}(\Delta f(r))\right) \tag{66}$$

So, by combining Eqs. 59, 60 and 66 with Eq. 58, we obtain the following relationship :

$$\pi RZG\left(R - \frac{\partial h(R)}{\partial r} - \frac{\partial}{\partial r}(\Delta f(r))\right) = 0 \tag{67}$$

We finally obtain a fifth boundary condition :

$$R - \frac{\partial h(R)}{\partial r} - \frac{\partial}{\partial r}\left(\Delta f(R)\right) = 0 \tag{68}$$

To summarize, at the inclusion frontier, we have set two new boundary conditions. First for velocity which is given by Eq.57 and the second for the stress on the inclusion which is given by Eq. 68.

2.2.7. Boundary conditions related to the energy conservation

Boundary conditions related to the energy conservation are determinated for both visco-inertial and thermal effects. A preliminary operation is performed on the Navier-Stokes Equation 19 which governs the fluid's movements on local scale. For practical reasons, it is written in the following useful form :

$$\mu\Delta\mathbf{v}(r) - j\omega\rho_0\mathbf{v}(r) = \nabla p \tag{69}$$

Then, the variational formulation method used previously in Section 2.1.4 is applied to Eq 69. However, instead of performing the scalar product by a $\mathbf{w}$ field, the local velocity conjugate $\overline{\mathbf{v}}$ is used. Thus the following relationship is obtained :

$$\mu \iiint_{\Omega_f} \Delta\left(\mathbf{v}(r)\right)\cdot\overline{\mathbf{v}}(r)\mathrm{d}\Omega - j\omega\rho_0 \iiint_{\Omega_f} \mathbf{v}(r)\cdot\overline{\mathbf{v}}(r)\mathrm{d}\Omega = \iiint_{\Omega_f} \nabla p\cdot\overline{\mathbf{v}}(r)\mathrm{d}\Omega \tag{70}$$

Now, it is possible to simplify Eq. 70 by using the flow-divergence theorem (Eq. 10) and by replacing $(\nabla.\mathbf{v}(r))$ with $2\underline{\mathbf{D}}(\mathbf{v}(r))$. Thus, the first term of Eq. 70 can be written :

$$2\mu \iiint_{\Omega_f} \left(\nabla\left(\underline{\mathbf{D}}\left(\mathbf{v}(r)\right)\right)\cdot\overline{\mathbf{v}}(r) + \underline{\mathbf{D}}\left(\mathbf{v}(r)\right)\cdot\underline{\mathbf{D}}\left(\overline{\mathbf{v}}(r)\right)\right)\mathrm{d}\Omega = 2\mu \oiint_{\partial\Omega} \underline{\mathbf{D}}\left(\mathbf{v}(r)\right)\overline{\mathbf{v}}(r)\cdot\mathbf{dS} \tag{71}$$

The right-hand term of Eq. 70 can be written as :

$$\iiint_{\Omega_f} \nabla p\cdot\overline{\mathbf{v}}(r)\mathrm{d}\Omega = \oiint_{\partial\Omega} p\overline{\mathbf{v}}(r)\cdot\mathbf{dS} \tag{72}$$

Now, Eq. 70 can be written as follows :

$$\begin{aligned} 2\mu \iiint_{\Omega_f} \underline{\mathbf{D}}\left(\mathbf{v}(r)\right)\cdot\underline{\mathbf{D}}\left(\overline{\mathbf{v}}(r)\right)\mathrm{d}\Omega + j\omega\rho_0 \iiint_{\Omega_f} \mathbf{v}(r)\cdot\overline{\mathbf{v}}(r)\mathrm{d}\Omega \\ = -\oiint_{\partial\Omega} p\overline{\mathbf{v}}(r)\cdot\mathbf{dS} + 2\mu \oiint_{\partial\Omega} \underline{\mathbf{D}}\left(\mathbf{v}(r)\right)\overline{\mathbf{v}}(r)\cdot\mathbf{dS} \end{aligned} \tag{73}$$

Eq. 73 can be related to Eq. 11 established previously by the HPM method. In order to adapt it to the SCM_{cyl} case, it can be written again by the following relation :

$$2\mu \iiint_{\Omega_f} \underline{\mathbf{D_y}}\left(\mathbf{v}(r)\right) \cdot \underline{\mathbf{D_y}}\left(\overline{\mathbf{v}}(r)\right) \mathrm{d}\Omega + j\omega\rho_0 \iiint_{\Omega_f} \mathbf{v}(r) \cdot \overline{\mathbf{v}}(r) \mathrm{d}\Omega = -\frac{1}{\mu} \nabla_{\mathbf{x}} P \iiint_{\Omega_f} \overline{\mathbf{v}}(r) \mathrm{d}\Omega \tag{74}$$

This relationship depicts the energy conservation between the local scale inclusion (left-hand terms) and the equivalent homogeneous medium at the macroscopic scale (right-hand term). By analogy between Eqs. 73 and 74, the following relationship can be established :

$$-\oiint_{\partial\Omega} p\overline{\mathbf{v}}(r) \cdot \mathbf{dS} + 2\mu \oiint_{\partial\Omega} \underline{\mathbf{D}}\left(\mathbf{v}(r)\right) \overline{\mathbf{v}}(r) \cdot \mathbf{dS} = -\nabla P \iiint_{\Omega_f} \overline{\mathbf{v}}(r) \mathrm{d}\Omega \tag{75}$$

By using the flow-divergence theorem on the right-hand term of Eq. 75, we finally obtain the following relationship :

$$-\oiint_{\partial\Omega} p\overline{\mathbf{v}}(r) \cdot \mathbf{dS} + 2\mu \oiint_{\partial\Omega} \underline{\mathbf{D}}\left(\mathbf{v}(r)\right) \overline{\mathbf{v}}(r) \cdot \mathbf{dS} = -\oiint_{\partial\Omega} P\overline{\mathbf{v}}(r) \cdot \mathbf{dS} \tag{76}$$

In order to express the energy equivalence between the inclusion and the same volume of the equivalent homogeneous medium, the approach previously used for boundary stress conditions is implemented. So, $\overline{\mathbf{V}}(R)$ is defined as the conjugate of the mean velocity at the frontier between the inclusion and the equivalent homogeneous medium. Then, the energy equivalence at $r = R$ can be written by the following relationship :

$$-\oiint_{\partial\Omega} \left[(P-p) + 2\mu\underline{\mathbf{D}}\left(\mathbf{v}(R)\right)\right] \cdot \left[\overline{\mathbf{v}}(R) - \overline{\mathbf{V}}(R)\right] \mathrm{d}S\mathbf{e_r} = \mathbf{0} \tag{77}$$

By doing the scalar product with $\mathbf{e_r}$, we get two relationships :

$$\begin{cases} -\oiint_{\partial\Omega} \left[(P-p) + 2\mu D_{rr}\right] \left[\overline{v_r}(R) - \overline{V_r}(R)\right] \mathrm{d}S & (78) \\ = 0 & (79) \\ -\oiint_{\partial\Omega} 2\mu D_{r\theta} \left[\overline{v_\theta}(R) - \overline{V_\theta}(R)\right] \mathrm{d}S = 0 & (80) \end{cases}$$

We saw previously that $\overline{v_r}(R) = \overline{V_r}(R)$, so Eq. 79 does not lead to the energy conservation conditions. On the other hand, Eq. 80 allows two possible condi-

tions. Indeed, either $\left[\overline{v_\theta}(R) - \overline{V_\theta}(R)\right]$, or $2\mu D_{r\theta} = 0$. In the first case, by expressing $v_\theta(R)$ from Eq. 49 and $V_\theta(R)$ from generalized Darcy equation (Eq. 17), we get the following relationship :

$$v_\theta(R) - V_\theta(R) = -\frac{\partial^2 f(R)}{\partial r^2}\frac{\mathbf{G}\cdot\mathbf{e}_\theta}{\mu} + \Pi\frac{\mathbf{G}\cdot\mathbf{e}_\theta}{\mu} \tag{81}$$

So, we obtain :

$$\frac{\partial^2 f(R)}{\partial r^2} = \Pi \tag{82}$$

Combining this result with the velocity boundary condition at the inclusion frontier, given by Eq.57, we finally obtain a sixth boundary condition relationship :

$$-\frac{1}{2}\Delta(f(R)) + \Pi = 0 \tag{83}$$

In this case, at the frontier between the inclusion and the equivalent homogeneous medium, the fluid phase velocity is equal to the velocity of the equivalent medium (radial and orthoradial components). On the other hand, there is no equality between the pressure in the inclusion and the pressure of the equivalent homogeneous medium. This kind of configuration has been named *flow approach* [32], it is noted hereafter with the v index. In the second case, by using the $D_{r\theta}$ expression, given by Eq. 64, we get an alternative boundary condition related to the energy conservation. It can be written by the following relationship :

$$\frac{\partial^3 f(R)}{\partial r^3} = \frac{1}{R}\frac{\partial^2 f(R)}{\partial r^2} = 0 \tag{84}$$

In this case, the shear stress is cancelled. Thus, the stress $(-p\mathbf{I} + 2\,\mu\,\underline{\mathbf{D}}(\mathbf{v}(R)))$ on the inclusion is equal to the pressure P in the equivalent homogeneous medium. However, at the frontier between the inclusion and the equivalent homogeneous medium the orthoradial velocities of the fluid phase and the homogeneous medium are not equal. This configuration is called *pressure approach* and it is written with the p index.

As for the visco-inertial case, the first step for the determination of the boundary condition related to thermal effect consists in applying the variational

formulation to the heat equation (Eq 22). To do that, $\overline{T}$ is used. So, the following relationship is obtained :

$$-\lambda_f \iiint_{\Omega_f} \Delta T(r)\overline{T}(r)\mathrm{d}\Omega + j\omega\rho_0 C_p \iiint_{\Omega_f} T(r)\overline{T}(r)\mathrm{d}\Omega = j\omega P \iiint_{\Omega_f} \overline{T}(r)\mathrm{d}\Omega \tag{85}$$

By applying the flow-divergence theorem to the first term of Eq. 85, we get the following relationship :

$$\lambda_f \iiint_{\Omega_f} \nabla T(r)\cdot\nabla\overline{T}(r)\mathrm{d}\Omega + j\omega\rho_0 C_p \iiint_{\Omega_f} T(r)\overline{T}(r)\mathrm{d}\Omega - \lambda_f \oiint_{\partial\Omega} \nabla T(r)\overline{T}(r)\mathbf{dS} = j\omega P \iiint_{\Omega_f} \overline{T}(r)\mathrm{d}\Omega \tag{86}$$

At the inclusion frontier ($r = R$), by identifying the Eq 86 with the previously established Eq. 14, we get the following relationship :

$$\lambda_f \oiint_{\partial\Omega} \nabla T(R)\overline{T}(R)\mathbf{dS} = 0 \tag{87}$$

It can also be written :

$$\lambda_f \frac{\partial T(R)}{\partial r}\overline{T}(R)\int_0^Z \mathrm{d}z \int_0^{2\pi} \mathrm{d}\theta = 0 \tag{88}$$

The first possibility is $\overline{T}(R)$ =0, but it is an artificial term used to apply the variational formulation, so that does not make physical sense. The second solution is $\frac{\partial T(R)}{\partial r} = 0$. Taking the T expression given by the Eq 42, we can finally write the boundary condition for the energy conservation of the thermal dissipation effects by the following relationship :

$$\frac{\partial \xi(R)}{\partial r} = 0 \tag{89}$$

Now, it is possible to determine all the constants for both pressure p and velocity v approaches. For each of them, we have 7 unknown constants c_0, c_1, c_2, c_3, c_4, c_5 and Π (v or p) for 7 equations. To summarize, the both equation systems are related to the following relationships :

- v-approach : Eqs. 46, 50, 51, 57, 68, 83 and 89 ;
- p-approach : Eqs. 46, 50, 51, 57, 68, 84 and 89.

2.2.8. Solutions for the SCM_{cyl} modeling method

The solving of these systems leads to the expressions of both visco-inertial and thermal permeabilities. To simplify the writing of the equations, four adimensional parameters are defined $p = \frac{r}{\delta_v}$, $q = p\,\beta$, $p' = \frac{r}{\delta_t}$ and $q' = p'\,\beta$. To solve the equation systems, a formal calculation software has been used. So, the visco-inertial permeabilities for both v and p approaches are given by the following relationships :

— v-approach :

$$\Pi_v = \delta_v^2 \left(\frac{R^2\phi A_0 + 2\delta_v R(\beta A_1 + A_2)}{R^2(1-\phi)A_0 + 2\delta_v(-2R\beta^2 A_3 + R\beta A_4 + RA_2 + 8\beta\delta_v A_5)} \right) \tag{90}$$

with A_0, A_1, A_2, A_3, A_4 and A_5 functions expressed by the following relationships :

$$\begin{cases} A_0 = I_0(p)K_0(q) - I_0(q)K_0(p), & (91) \\ A_1 = I_0(p)K_1(q) - I_0(q)K_1(q) + I_1(q)K_0(p) - I_1(q)K_0(q), & (92) \\ A_2 = I_0(p)K_1(p) - I_0(q)K_1(p) + I_1(p)K_0(p) - I_1(p)K_0(q), & (93) \\ A_3 = I_0(q)K_1(p) + I_1(p)K_0(q), & (94) \\ A_4 = I_0(p)K_1(q) + I_0(q)K_1(q) + I_1(q)K_0(p) + I_1(q)K_0(q), & (95) \\ A_5 = -I_1(p)K_1(q) + I_1(q)K_1(p) & (96) \end{cases}$$

— p-approach :

$$\Pi_p = \delta_v^2 \left(\frac{R^3\phi A_3 + R^2\delta_v(2\beta A_5 - \phi A_0) + 2\delta_v^2 R(\beta A_1 - A_2)}{\phi R^3 A_3(R^2 + 4\beta^2\delta_v) - R^2\delta_v(2-\phi)A_0 - 2R\delta_v^2(A_2 + \beta A_4) - 2\beta\delta_v(R^2 + 4\delta_v^2)A_5} \right) \tag{97}$$

The A_0, A_1, A_2, A_3, A_4 and A_5 functions are the same as for v-approach. There are expressed by Eqs. 91, 92, 93, 94, 95 and 96.

The thermal permability is given by the following relationship :

$$\Xi(\omega) = \delta_t^2 \left(1 - \frac{2\delta_t^3}{R\phi A_6} \left[A_7 - A_8 \right] \right) \tag{98}$$

with A_6, A_7 and A_8 functions expressed by the following relationships :

$$\begin{cases} A_6 = I_0(q')K_1(p') + K_0(q')I_1(p'), & (99) \\ A_7 = K_1(p')(\beta I_1(q') - I_1(p')), & (100) \\ A_8 = I_1(p')(\beta K_1(q') - K_1(p')), & (101) \end{cases}$$

Then, by associating each dynamic visco-inertial permeability (Π_v or Π_p) with the thermal permeability (Ξ), it is possible to get both parameter couples : (ρ_v,K) or (ρ_p,K). Finally, we can get two possible sound absorption coefficients α_v or α_p. To summarize, based on both a mean fibre radius and a porosity value, the SCM_{cyl} method developed in this paper leads to two possible solutions :

— v-approach $\Rightarrow (\Pi_v, \Xi) \Rightarrow (\rho_v, K) \Rightarrow \alpha_v$

— p-approach $\Rightarrow (\Pi_p, \Xi) \Rightarrow (\rho_p, K) \Rightarrow \alpha_p$.

3. Validation and discussion

In this section, the SCM_{cyl} method is validated by comparison with experimental measurements. Two vegetal wools are characterized at microscopic scale to obtain modeling approach input parameters as well as at macroscopic scale to measure their sound absorption properties. Finally, the approach developed in this paper is discussed.

3.1. Materials

Both materials used for the validation of the SCM_{cyl} modeling approach are thermobonded vegetal wools manufactured as a single panel with one kind of vegetal fibres over its entire thickness. The first one is a flax wool (refered as "Flax") and the second one is a hemp wool (refered as "Hemp"). These both types of fibrous materials have been chosen because they are among the most widely used biobased insulation materials in green buildings. The both vegetal wools are shown in FIG 3. As shown in Table 1, the both materials have relatively different thickness and bulk density values to lead to different sound absorption coefficients. These wools characteristics are based on 5 measurements for every 4 samples of each material.

3.2. Methods

3.2.1. Fibre size distribution

Microstructure pictures of the wools have been realized using a FEI Quanta 400 Scanning Electron Microscope (SEM) in secondary electron (SE) imaging

(a) (b)

FIGURE 3: The materials, (a) "Flax", (b) "Hemp"

mode in low vacuum. Then, these pictures are analysed to characterize the vegetal fibre specificities. As shown in FIG 4 (a), vegetal fibres are present either in the form of a single fibre or fibre bundles. However, due to the 2D nature of the images and the great variability in the vegetal fibre shapes and morphologies, it is generally difficult to really distinguish them. Thus, in the following of this paper, as a first approach, all characterized elements will be assimilated to fibres and represented by a fibre radius value. Although fibres are not perfectly circular, it is assumed that they can be considered as cylinders of constant radius over their entire length, as shown in FIG 4 (a). This hypothesis is corroborated by the results carried out in [47] for which the circularity of flax fibres had been estimated at 0.907. To determine the fibre radii distribution, we rely on the works carried out in [8, 13, 48, 49]. So, using Mesurim © software, the measurements are performed by drawing a transversal segment to the longitudinal axis of the fibre, as shown in Fig. 4 (b).

In order to comply with these work recommendations, for each material, at least 300 fibre diameters are recorded from a minimum of 20 pictures. The

Material	Thickness (mm)	Bulk density ($kg.m^{-3}$)	Porosity (%)	Mean fibre radius (μm)
Flax	48 ± 1	26.6 ± 1.1	98.4 ± 0.2	11.8 ± 1.6
Hemp	107 ± 2	40.8 ± 2.7	97.4 ± 0.2	16.7 ± 1.7

TABLE 1: Experimental characteristics of the vegetal wools obtained under a thermal condition of $T = 25 \pm 0.8^{\circ}C$ and a relative humidity of $RH = 40 \pm 2\%$. Data are presented with mean value $\pm$

standard deviation.

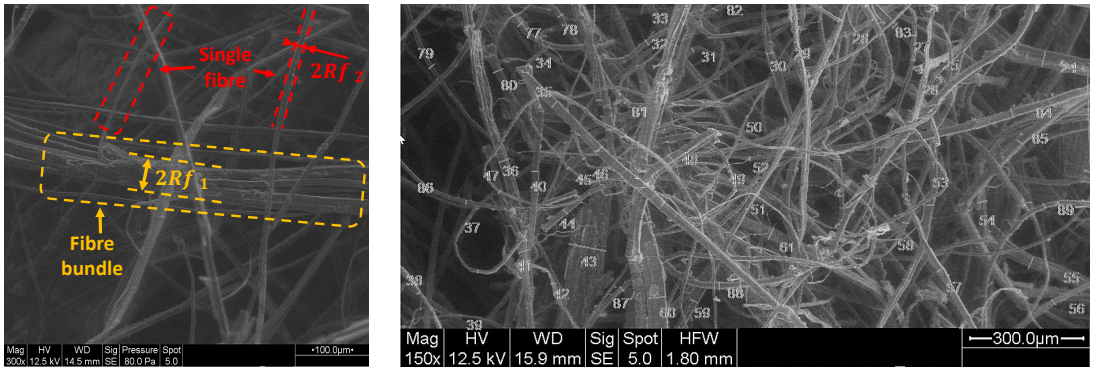

(a) (b)

FIGURE 4: Analysis and exploitation of SEM pictures, (a) flax single fibres and fibre bundle, (b) radius measurements of hemp wool fibres with Mesurim © software

measured fibre radius distributions for flax and hemp wools are represented by bar charts as shown in Fig. 5. The smallest measured fibres have radii of approximately $3\mu m$. For the biggest ones, radii values are around $80\mu m$ for the hemp fibres and around $90\mu m$ for the flax fibres. Although the bar charts are relatively similar, the distribution of hemp fibre radii shows more elements above $30\mu m$. On the other hand, as shown in Fig. 5, these are log-normal laws which better correspond to the vegetal fibre radii distributions. Nevertheless, as the SCM_{cyl} modeling approach is based on an equivalent fiber radius value, in a first approach, we choose a single radius value corresponding to the mean of the fibre radii [3, 8, 13, 48]. In [23, 28] the fibre radius is weighted according

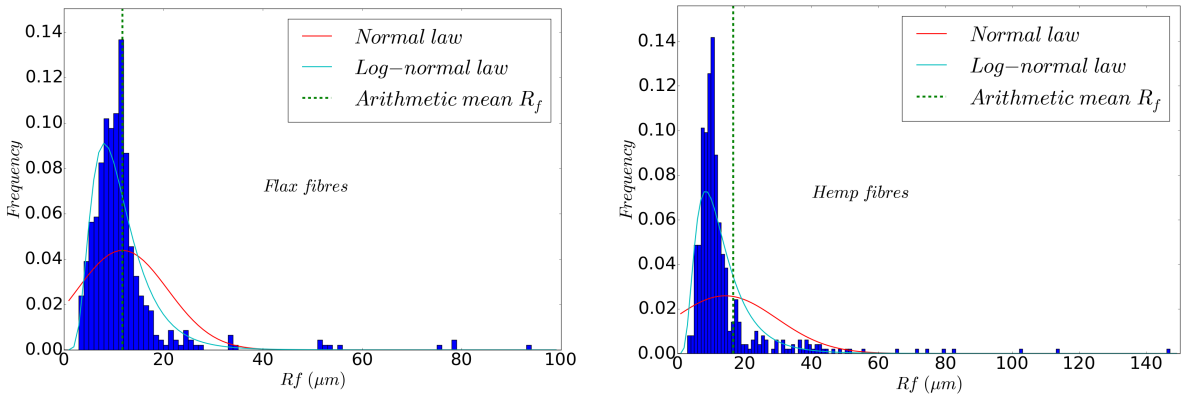

(a) (b)

FIGURE 5: Bar charts of fibre radii distributions, (a) flax wool, (b) hemp wool

to its corresponding fibre volume. This typically shifts the single fibre radius towards larger values. However, in our case, as the length of the fibres is not known, it is not possible to apply this correction. Moreover, as shown in Fig. 5, for both distributions, the arithmetic mean fibre radii value is greater than the mean radii value related to the log-normal laws. Indeed, the arithmetic mean better takes the influence and the presence of large size elements into account.

The results are presented in Table 1.

3.2.2. Porosity

The porosity was experimentally characterized using the air volumes comparison method described in [50]. This method leads to the determination of the porosity directly accessible by air. It corresponds to the open porosity of materials by determining directly the volume of their solid phase. Both the inter-fibre porosity and the open intra-fibre porosity can be considered as the accessible porosity of vegetal wools. Nevertheless, works carried out in [5] have estimated that the intra-fibre porosity is lower than 0.2% of the total porosity for this type of material. So, as a first approach, it can be neglected.

The results presented in Table 1 were obtained from five measurements on both materials.

3.2.3. Sound absorption coefficient

A B&K © type 4106 standing wave tube with an inner diameter of 100 mm, was used to experimentally characterize the sound absorption coefficient of the both sides of four samples for each vegetal wool. These measurements were carried out at normal incidence according to standard ISO 10534-2 [51]. Taking the configuration of the impedance tube and the distance between the two microphones located upstream of the sample (7.5 cm) into account, the standard ISO 10534-2 leads to a validity limit value for low-frequency measurements of 226Hz.The validity limit of high-frequency measurements is estimated to be around 2000Hz. The three position method without cavity, based on the work carried out in [52] and adapted by [53] for microphones located outside the tube, was used. This method leads to the determination of intrinsic material parameters, the bulk modulus (K) and the dynamic density (ρ).

3.3. Modeling validation

In a first step, the both dynamic density SCM_{cyl} modeling, ρ_v and ρ_p, are compared to the experimental ones. Then, in the same way, the bulk modulus (K_{exp} and K_{SCM}) obtained by both experimental measurements and SCM_{cyl} modeling method are analyzed. Finally, the sound absorption coefficients (α_v and α_p) based on materials thickness, dynamic densities and bulk modulus are modelized and compared to the experimental measurements.

3.3.1. Dynamic densities

For visco-inertial effects, the real and the imaginary parts of the normalized dynamic density (ρ/ρ_0) of the experimental measurements and both SCM_{cyl} modeling approaches for the both vegetal wools are shown in Fig. 6. As expected for the both materials, Fig. 6 shows that both approaches give values of the real part of the dynamic density close to 1 regardless of the frequency. For the imaginary part, in a classic way, both modeling approaches of materials follow a trend in $-\frac{\sigma}{\omega}$ for low frequency and close to 0 when the frequency increases, as shown by Fig. 6. It should be noted that the differences between ex-

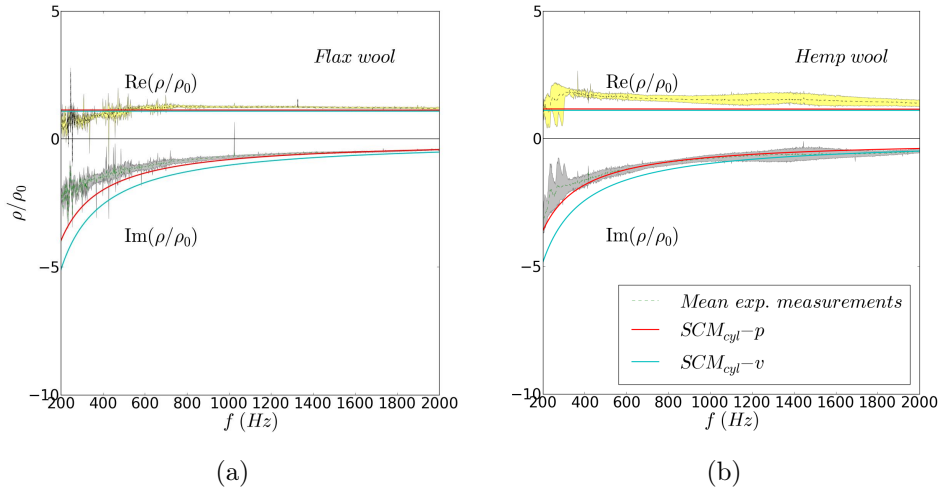

(a) (b)

FIGURE 6: Experimental characterisation and SCM_{cyl} modeling of the normalised dynamic density as a function of frequency for (a) the flax wool and (b) the hemp wool

perimental and modeling results in the low-frequency regime for the imaginary part of the normalized dynamic density are slightly larger for flax wool than for hemp wool. This is confirmed by the airflow resistivity values determined by the low-frequency limit from both experimental measurements and SCM_{cyl} modeling. Indeed, for flax wool we obtain $\sigma_{exp} = 4161 N.m^{-4}.s$, $\sigma_p = 5008 N.m^{-4}.s$ and $\sigma_v = 6432 N.m^{-4}.s$, while the differences are smaller for hemp wool with $\sigma_{exp} = 3993 N.m^{-4}.s$, $\sigma_p = 4611 N.m^{-4}.s$ and $\sigma_v = 6062 N.m^{-4}.s$. For these both materials, no significant limp behaviour was observed. If so, the SCM modeling could have been mixed with the dynamic density related to a limp behaviour [54, 55]. However, a difference is observed between the curves of the both approaches. Indeed, for both materials, the flow approach is slightly further away than the pressure approach. This trend follows the same behaviour already observed for spherical modeling. The cause of the differences between the results of the flow and pressure approaches requires further investigation.

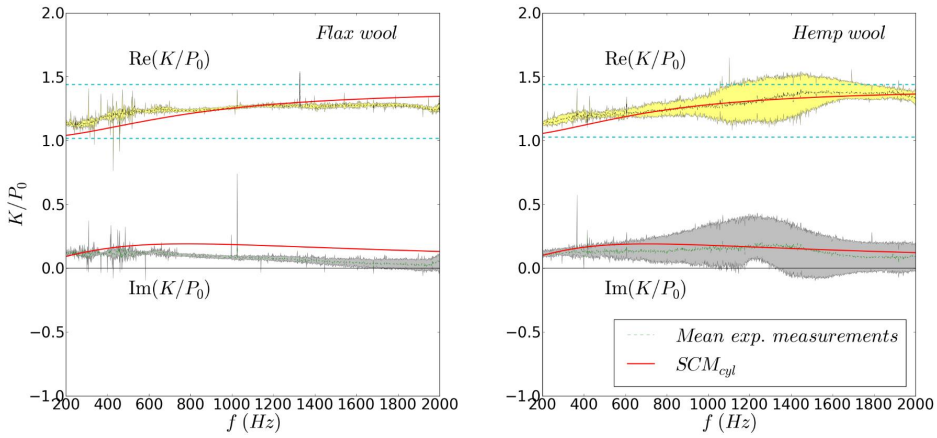

FIGURE 7: Experimental characterisation and SCM_{cyl} modeling of the normalised bulk modulus as a function of frequency for (a) the flax wool and (b) the hemp wool

3.3.2. Bulk modulus

For thermal effects, Fig. 6 shows both real and imaginary parts of the normalized bulk modulus (K/P_0) obtained by the experimental measurements and the SCM_{cyl} modeling approach for the both wools. For the real part of this parameter, the modeling method remains between the two physical limit values corresponding to $\mathrm{Re}(K/P_0) \simeq 1/\phi$ in low frequency (isothermal regime) and $\mathrm{Re}(K/P_0) \simeq \gamma/\phi$ in high frequency (adiabatic regime). Thus, it is verified that when the frequency is low ($f \rightarrow 0$), the real part of the normalized bulk modulus from SCM_{cyl} modeling tends towards $1/\phi$. Concerning the imaginary part of the normalized bulk modulus, as expected, at low frequency we have $\lim_{f\rightarrow 0} \mathrm{Im}(K/P_0) = 0$. Then it increases to the thermal transition frequency before decreasing again to zero. For both materials, as shown by Fig. 7, the SCM_{cyl} modeling approach is relatively close to the experimental measurements.

3.3.3. Sound absorption coefficient

The results of the SCM_{cyl} modeling, shown in Fig. 8, are relatively close to the experimental measurements for both materials. In both cases, the pressure

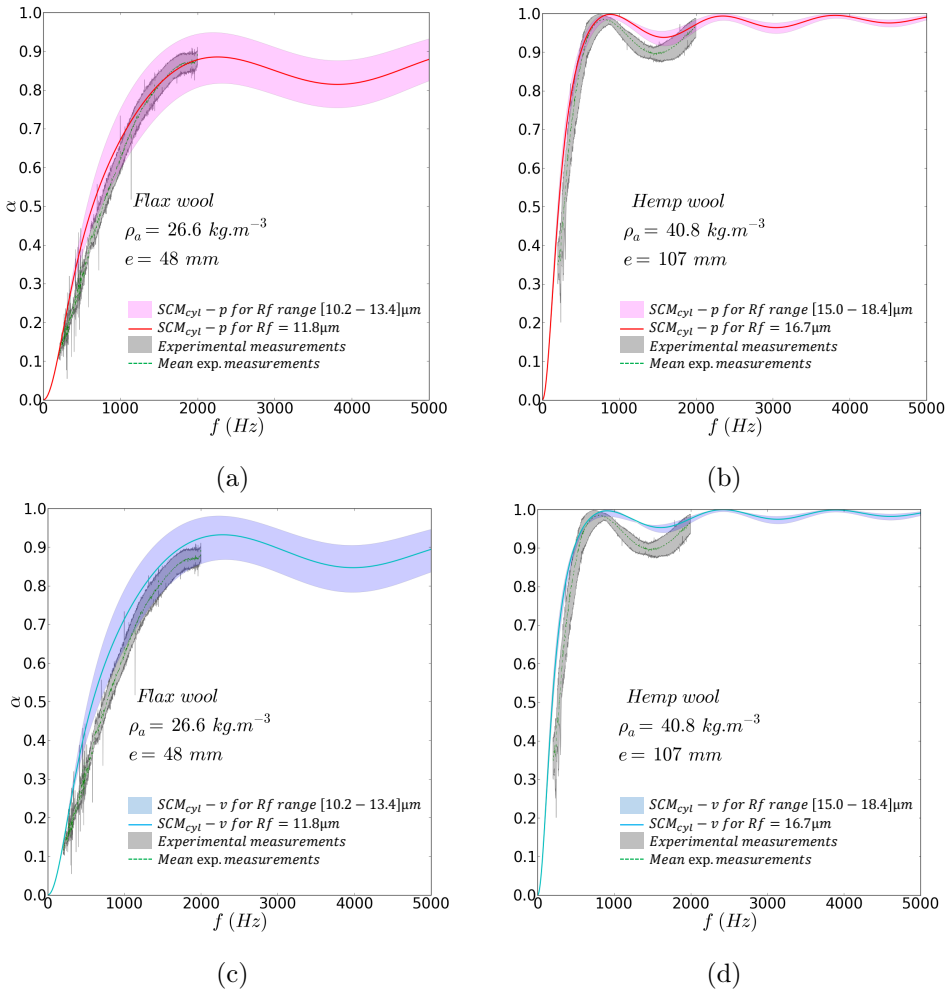

FIGURE 8: Experimental characterisation and modeling of the sound absorption coefficient as a function of frequency for (a) the flax wool and the $SCM_{cyl} - p$ modeling, (b) the hemp wool and the $SCM_{cyl} - p$ modeling, (c) the flax wool and the $SCM_{cyl} - v$ modeling and (d)the hemp wool and the $SCM_{cyl} - v$ modeling

approach has a lower mean relative deviation than the experimental relative deviation, as shown in Table 2. Indeed, both values are less than 10%. In the both cases, the flow approach is slightly further away than the pressure approach. As shown in Table 2, for the hemp wool, the relative deviation is less than 10%, but for the flax wool, it is higher but remains close to the experimental mean

deviation.

Material	Exp. mean relative deviation (%)	Mean relative deviation (%)	
		p	v
Flax	11.8	9.4	16.1
Hemp	11.7	6.4	8.9

TABLE 2: Relative deviation of the experimental measurements and mean relative deviation between SCM_{cyl} modeling and mean experimental values.

So, both $SCM_{cyl} - p$ and $SCM_{cyl} - v$ modeling approaches developed in this paper can be validated in order to determine sound absorption coefficient of vegetal wools.

On the other hand, the sound absorption deviation as a function of fibre radii dispersion (values are indicated in Table 1) is shown in Fig. 8. It gives an overview of the SCM_{cyl} modeling sensitivity regarding the fiber radius value, which is a key input parameter, in these two particular cases. The results are similar for both pressure and flow approaches, but are different for each material. In our case, where the both materials have equivalent airflow resistivities, the sensitivity decreases as the thickness of the material increases. However, this result would require a more systematic study in order to better understand the relationship between the modeling sensitivity and parameters such as fibre radius, porosity, airflow resistivity, material thickness etc. Finally, by using both sound absorption coefficient and porosity values, both of these modeling approaches can also be used to obtained an equivalent fibre radius for a fibrous material or more precisely, a range of fibre radii to be consistent with the previous result.

3.4. Limits and outlooks about the SCM_{cyl} approaches

A huge benefit of the SCM_{cyl} method developed here is that it is based on only two parameters, a porosity value and a mean fibre radius. However, vegetal wools are often made up of other fibre types that may have different radii. So, to take a second fibre type into account, it is possible to mix the SCM_{cyl} modeling

method with a composite modeling approach as in [8]. This modeling approach has been elaborated to describe materials including two types of microstructures. In the case of vegetal wools, the material is considered as a mixture of two fibrous media represented by a volume fraction of polymer fibres within vegetal ones. Moreover, in order to better model the behaviour of vegetal wools, it might also be relevant to take the variability of vegetal fibre distributions into account, using the whole size distribution of materials. Indeed, it could lead in extreme cases to double porosity effects as shown in [56] for hemp particles. In this paper, the choice has been done to develop the SCM_{cyl} modeling with a focus only on the specific case of a perpendicular sound propagation. However, it would also be relevant to take a mix of both perpendicular and parallel sound propagation into account in the modeling approach. Indeed, during the manufacturing process, the fibres are not always arranged in regular parallel layers and may have a low inclination. Finally, the SCM_{cyl} modeling method has been validated for a frequency range specific to the building field. Nevertheless, it also seems relevant to study the low and high frequency limits of both visco-inertial and thermal permeabilities (Π and Ξ) using the SCM_{cyl} relationships. It would then be possible to relate the SCM_{cyl} modeling approaches to the specific parameters of the fluid-equivalent models used for porous materials.

4. Conclusion

In this paper, a self-consistent modeling approach for the sound absorption properties of fibrous materials has been developed. It is called SCM_{cyl}. By using HPM, it is based on the rigorous establishment of macroscopic behaviour laws for fluid flow relating to the dissipation phenomena of visco-inertial and thermal effects. In order to establish analytical relationships between specific microscale fibrous parameters with their macroscopic properties, assumptions are made to represent the microstructure as a generic cylindrical inclusion (a solid phase included in a fluid phase) which is close to the fibre morphology. So, the development of the SCM_{cyl} modeling led to equations for both the dynamic

density ρ and the bulk modulus K. For ρ two possible solutions are obtained : a velocity approach $\rho - v$ and a pressure approach $\rho - p$. Finally, both $SCM_{cyl} - v$ and $SCM_{cyl} - p$ approaches lead to a useful sound absorption modeling based on only two input parameters : a porosity value (ϕ) and a mean fibre radius (Rf). These approaches has been validated for the vegetal wools case by showing a fit between both $SCM_{cyl} - v$ and $SCM_{cyl} - p$ modeling predictions with experimental measurements. It is also possible to reverse the SCM_{cyl} modeling in order to obtain an equivalent fibre radius value by using a porosity and a sound absorption coefficient values. Nevertheless, it is necessary to take the dispersions related to the used parameters into account in this inversion. In order to extend the field of use, the modeling approaches developed here can be applied to other fibrous materials and even to the case of materials that can be represented by cylindrical geometries and subjected to flow propagation. Finally, future work may also investigate the possibility of joint approaches with SCM modeling methods developed for the determination of the fibrous materials thermal properties.

Acknowledgements

This work was performed within the framework of the LABEX CeLyA (ANR-10-LABX-0060) of Université de Lyon, France. Moreover, the authors thank Laroche S.A. and CAVAC Biomatériaux companies for providing the materials of this study.

References

[1] G. Lumia, Bio-based insulation materials : an opportunity for the renovation of European residential building stock. Evaluation of carbon uptake benefits through a dynamic life cycle assessment (DLCA), Ph.D. thesis (2017).

[2] F. Pittau, F. Krause, G. Lumia, G. Habert, Fast-growing bio-based materials as an opportunity for storing carbon in exterior walls, Building and En-

vironment 129 (2018) 117–129. doi:10.1016/j.buildenv.2017.12.006.
URL https://linkinghub.elsevier.com/retrieve/pii/S0360132317305644

[3] D. Oldham, C. Egan, R. Cookson, Sustainable acoustic absorbers from the biomass, Applied Acoustics 72 (6) (2011) 350–363. doi:10.1016/j.apacoust.2010.12.009.
URL http://linkinghub.elsevier.com/retrieve/pii/S0003682X10002914

[4] F. Asdrubali, S. Schiavoni, K. Horoshenkov, A review of sustainable materials for acoustic applications, Building Acoustics 19 (4) (2012) 283–312.

[5] P. Glé, Acoustics of building materials based on plant fibers and particules : Tools for characterization, modelling and optimisation, Ph.D. thesis, INSA de Lyon (2013).

[6] U. Berardi, G. Iannace, Acoustic characterization of natural fibers for sound absorption applications, Building and Environment 94 (2015) 840–852. doi:10.1016/j.buildenv.2015.05.029.
URL http://linkinghub.elsevier.com/retrieve/pii/S036013231530007X

[7] J. P. Arenas, F. Asdrubali, Eco-Materials with Noise Reduction Properties, in : L. M. T. Martínez, O. V. Kharissova, B. I. Kharisov (Eds.), Handbook of Ecomaterials, Springer International Publishing, Cham, 2018, pp. 1–26, dOI : 10.1007/978-3-319-48281-1_137-1.
URL http://link.springer.com/10.1007/978-3-319-48281-1_137-1

[8] C. Piégay, P. Glé, E. Gourdon, E. Gourlay, S. Marceau, Acoustical model of vegetal wools including two types of fibers, Applied Acoustics 129 (2018) 36–46. doi:10.1016/j.apacoust.2017.06.021.
URL http://linkinghub.elsevier.com/retrieve/pii/S0003682X17303274

[9] L. Lei, N. Dauchez, J. Chazot, Prediction of the six parameters of an equivalent fluid model for thermocompressed glass wools and melamine foam, Applied Acoustics 139 (2018) 44–56. doi:10.1016/j.apacoust.2018.04.010.
URL https://linkinghub.elsevier.com/retrieve/pii/S0003682X17305728

[10] C. Piégay, P. Glé, E. Gourdon, E. Gourlay, A cylindrical self-consistent modelling of vegetal wools thermal conductivity, Construction and Building Materials 232 (2020) 117123. doi:10.1016/j.conbuildmat.2019.117123.
URL https://linkinghub.elsevier.com/retrieve/pii/S0950061819325656

[11] C. Peyrega, D. Jeulin, Estimation of Acoustic Properties, of the representative Volume Element of Random Fibrous Media, Journal of Applied Physics, American Institute of Physics 113 (10) (2013) 104901–104901–13.

[12] K. Gao, J. van Dommelen, P. Göransson, M. Geers, A homogenization approach for characterization of the fluid–solid coupling parameters in Biotś equations for acoustic poroelastic materials, Journal of Sound and Vibration 351 (2015) 251–267. doi:10.1016/j.jsv.2015.04.030.
URL https://linkinghub.elsevier.com/retrieve/pii/S0022460X15003624

[13] H.-T. Luu, C. Perrot, R. Panneton, Influence of Porosity, Fiber Radius and Fiber Orientation on the Transport and Acoustic Properties of Random Fiber Structures, Acta Acustica united with Acustica 103 (6) (2017) 1050–1063. doi:10.3813/AAA.919134.
URL http://www.ingentaconnect.com/content/10.3813/AAA.919134

[14] M. Delany, E. Bazley, Acoustical properties of fibrous absorbent materials, Applied acoustics 3 (2) (1970) 105–116.
URL http://www.sciencedirect.com/science/article/pii/0003682X70900319

[15] Y. Miki, Acoustical properties of porous materials - Modifications of Delany-Bazley models, Journal of the Acoustical Society of Japan 11 (1) (1990) 19–24.

[16] R. Kirby, On the modification of Delany and Bazley fomulae, Applied Acoustics 86 (2014) 47–49. doi:10.1016/j.apacoust.2014.04.020.
URL https://linkinghub.elsevier.com/retrieve/pii/S0003682X14001261

[17] D.-L. Johnson, J. Koplik, R. Dashen, Theory of dynamic permeability and tortuosity in fluid-satured porous media, Fluid Mechanics 176 (1987) 379–402.

[18] Y. Champoux, J.-F. Allard, Dynamic tortuosity and bulk modulus in air-satured porous media, Applied Physics 70 (1991) 1975–1979.

[19] D. Lafarge, P. Lemarinier, J.-F. Allard, V. Tarnow, Dynamic compressibility of air in porous structures at audible frequencies, Journal of the acoustical Society of America 102 (4) (1997) 1995–2006.

[20] K. V. Horoshenkov, J.-P. Groby, O. Dazel, Asymptotic limits of some models for sound propagation in porous media and the assignment of the pore characteristic lengths, The Journal of the Acoustical Society of America 139 (5) (2016) 2463–2474. doi:10.1121/1.4947540.
URL http://asa.scitation.org/doi/10.1121/1.4947540

[21] A. Bensoussan, J. Lions, G. Papanicolaou, Asymptotic Analysis for Periodic Structures, Vol. 5, North Holland, 1978.

[22] E. Sanchez-Palencia, Non-homogeneous media and vibration theory, Vol. 127 of Lecture Notes in Physics, Springer-Verlag Berlin Heidelberg, 1980.

[23] C. Peyrega, Prédiction des propriétés acoustiques de matériaux fibreux hétérogènes à partir de leur microstructure 3d, Ph.D. thesis, Ecole Nationale des mines de Paris (2010).

[24] K. Gao, J. van Dommelen, P. Göransson, M. Geers, Computational homogenization of sound propagation in a deformable porous material including microscopic viscous-thermal effects, Journal of Sound and Vibration 365 (2016) 119–133. doi:10.1016/j.jsv.2015.11.037.
URL https://linkinghub.elsevier.com/retrieve/pii/S0022460X15009578

[25] C. Perrot, Microstructure et macro-comportement acoustique : approche par reconstruction d'une cellule élémentaire représentative, Ph.D. thesis, INSA de Lyon (2006).

[26] T. G. Zieliński, R. Venegas, C. Perrot, M. Červenka, F. Chevillotte, K. Attenborough, Benchmarks for microstructure-based modelling of sound absorbing rigid-frame porous media, Journal of Sound and Vibration (2020) 115441doi:10.1016/j.jsv.2020.115441.
URL https://linkinghub.elsevier.com/retrieve/pii/S0022460X2030273X

[27] C. Perrot, F. Chevillotte, R. Panneton, Bottom-up approach for microstructure optimization of sound absorbing materials, The Journal of the Acoustical Society of America 124 (2) (2008) 940–948. doi:10.1121/1.2945115.
URL http://asa.scitation.org/doi/10.1121/1.2945115

[28] M. He, C. Perrot, J. Guilleminot, P. Leroy, G. Jacqus, Multiscale prediction of acoustic properties for glass wools: Computational study and experimental validation, The Journal of the Acoustical Society of America 143 (6) (2018) 3283–3299. doi:10.1121/1.5040479.
URL http://asa.scitation.org/doi/10.1121/1.5040479

[29] H.-T. Luu, Multi-scale modeling of the sound dissipation in fabrics made of natural fibers, PhD Thesis, Université de Sherbrooke, Quebec, Canada (2016).

[30] Z. Hashin, Assessment of the self consistent scheme approximation : conduc-

tivity of particulate composites, J Compos Mater 2 (3) (1968) 284–300. doi:10.1177/002199836800200302.

[31] C. Boutin, Conductivité thermique du béton cellulaire autoclavé : modélisation par méthode auto-cohérente, Materials and Structures (29) (1996) 609–615. doi:10.1007/BF02485968.

[32] C. Boutin, C. Geindreau, Estimates and bounds of dynamic permeability of granular media, The Journal of the Acoustical Society of America 124 (6) (2008) 3576–3593. doi:10.1121/1.2999050.
URL http://asa.scitation.org/doi/10.1121/1.2999050

[33] C. Boutin, C. Geindreau, Periodic homogenization and consistent estimates of transport parameters through sphere and polyhedron packings in the whole porosity range, Physical review E 82 (3) (2010) 036313. doi:10.1103/PhysRevE.82.036313.

[34] C. Boutin, Study of permeability by periodic and self-consistent homogenisation, European Journal of Mechanics - A/Solids 19 (4) (2000) 603–632. doi:10.1016/S0997-7538(00)00174-1.

[35] A. Berdichevsky, Z. Cai, Perform permeability predictions by self consistent method and finite element simulation, Polym. Compos. 14 (2) (1993) 132–143. doi:10.1002/pc.750140207.

[36] O. Umnova, K. Attenborough, K. Ming Li, Cell model calculations of dynamic drag parameters in packings of spheres, Journal of Acoustical Society of America 107 (2000) 3113–3118.

[37] V. Tarnow, Airflow resistivity of models of fibrous acoustic materials, The Journal of the Acoustical Society of America 100 (6) (1996) 3706–3713.
URL http://scitation.aip.org/content/asa/journal/jasa/100/6/10.1121/1.417233

[38] V. Tarnow, Calculation of the dynamic air flow resistivity of fiber materials, The Journal of the Acoustical Society of America 102 (3) (1997) 1680–1688.

URL http://scitation.aip.org/content/asa/journal/jasa/102/3/10.1121/1.420079

[39] V. Tarnow, Compressibility of air in fibrous materials, Journal of the acoustical Society of America 102 (3) (1997) 1680–1688.

[40] T. Levy, Propagation of waves in fluid saturated porous elastic solid, The International Journal of Engineering Science (17) (1979) 1005–1014.

[41] J.-L. Auriault, Dynamic behaviour of a porous medium saturated by a newtonien fluid, International Journal of Ingineering Science 18 (6) (1980) 775–785. doi:10.1016/0020-7225(80)90025-7.

[42] T. G. Zieliński, Microstructure representations for sound absorbing fibrous media: 3D and 2D multiscale modelling and experiments, Journal of Sound and Vibration 409 (2017) 112–130. doi:10.1016/j.jsv.2017.07.047.
URL https://linkinghub.elsevier.com/retrieve/pii/S0022460X17305825

[43] M.-A. Biot, Theory of propagation of elastic waves in a fluid-saturated porous solid. I. low-frequency range, The Journal of the acoustical Society of america 28 (1) (1956) 168–178.

[44] M.-A. Biot, Theory of propagation of elastic waves in a fluid-saturated porous solid. II. Higher frequency range, The Journal of the acoustical Society of america 28 (2) (1956) 179–191.

[45] C. Zwikker, C.-W. Kosten, Sound Absorbing Materials, Elsivier Publishing Company, New-York, 1949.

[46] I. Howells, Drag due to the motion of a Newtonian fluid through a sparse random array of small fixed objects, Journal of Fluid Mechanics 64 (1974) 449–485.

[47] K. Charlet, J.-P. Jernot, J. Breard, M. Gomina, Scattering of morphological and mechanical properties of flax fibres, Industrial Crops and Products 32 (3) (2010) 220–224.

[48] P. Kerdudou, J.-B. Chéné, G. Jacqus, C. Perrot, S. Berger, P. Leroy, A semi-empirical approach to link macroscopic parameters to microstructure of fibrous materials, in : The 44th International Congress and Exposition on Noise Control Engineering (Inter-Noise2015), 2015.

[49] K. Singha, S. Maity, M. Singha, P. Paul, D. Gon, Effects of fiber diameter distribution of nonwoven fabrics on its properties, International Journal of Textile Science 1 (1) (2012) 7–14.
URL http://article.sapub.org/10.5923.j.textile.20120101.02.html

[50] P. Leclaire, O. Umnova, K. Horoshenkov, L. Maillet, Porosity measurement by comparison of air volumes, Review of Scientific Instruments 74 (3) (2003) 1366–1370. doi:10.1063/1.1542666.

[51] ISO 10534-2, NF EN ISO 10534-2 Janvier 2003 - Détermination du facteur d'absorption acoustique et de l'impédance des tubes d'impédance - Partie 2 : méthode de la fonction de transfert (2003).

[52] T. Iwase, Y. Izumi, R. Kawabata, A new measuring method for sound propagation constant by using sound tube without any air spaces back of a test material, Internoise 98, Christchurch, New Zealand (1998) 4.

[53] Y. Salissou, R. Panneton, Wideband characterisation of the complex wave number and characteristic impedance of sound absorbers, Journal of the acoustical Society of America 128 (5) (2010) 2868–2876.

[54] R. Panneton, Comments on the limp frame equivalent fluid model for porous media, The Journal of the Acoustical Society of America 122 (6) (2007) EL217–EL222. doi:10.1121/1.2800895.
URL http://asa.scitation.org/doi/10.1121/1.2800895

[55] O. Doutres, N. Dauchez, J.-M. Génevaux, O. Dazel, Validity of the limp model for porous materials: A criterion based on the Biot theory, The Journal of the Acoustical Society of America 122 (4) (2007) 2038–2048.

doi:10.1121/1.2769824.
URL http://asa.scitation.org/doi/10.1121/1.2769824

[56] P. Glé, E. Gourdon, L. Arnaud, K. V. Horoshenkov, K. Khan, The Effect of Particle Shape and Size Distribution on the Acoustical Properties of Mixtures of Hemp Particles, Journal of Acoustical Society of America 134 (6) (2013) 4698–4709. doi:10.1121/1.4824931.